# Versatile Recompression-Aware Perceptual Image Super-Resolution

Mingwei He<sup>1,2\*</sup>, Tongda Xu<sup>1\*</sup>, Xingtong Ge<sup>3</sup>, Ming Sun<sup>4</sup>, Chao Zhou<sup>4</sup>, Yan Wang<sup>1†</sup>
<sup>1</sup>AIR, Tsinghua University, <sup>2</sup>AGUS Tech, <sup>3</sup>HKUST, <sup>4</sup>Kuaishou Technology

mwhe@agus-tech.com, x.tongda@nyu.edu, wangyan@air.tsinghua.edu.cn

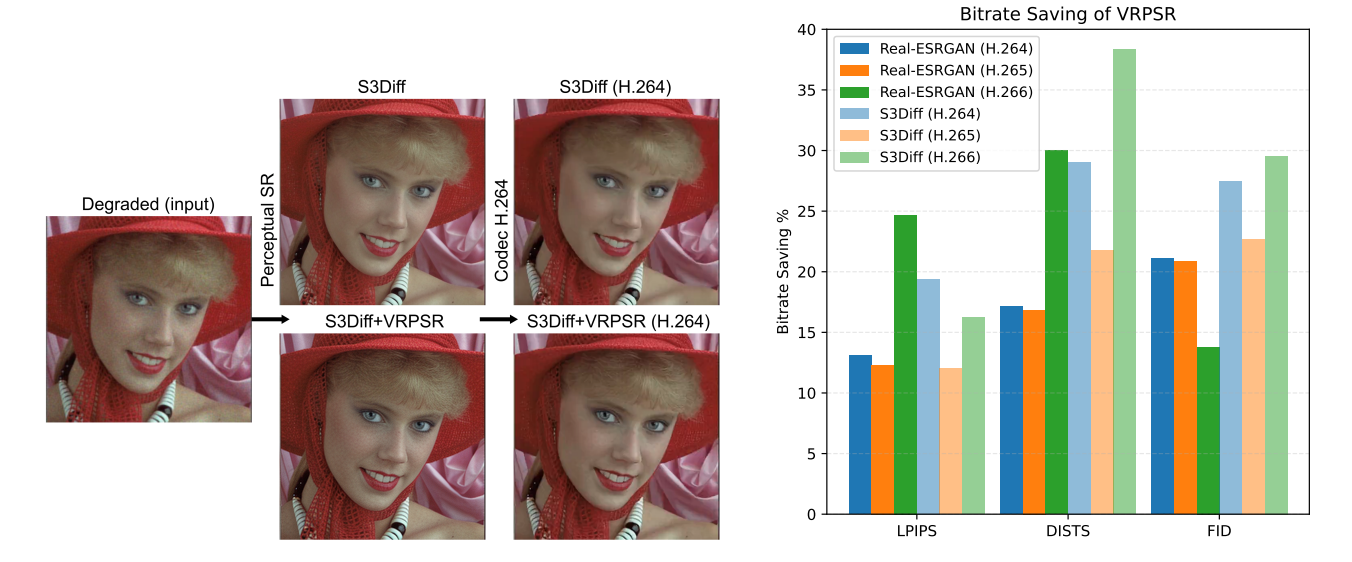


Figure 1. *left:* An example of recompression-aware perceptual super-resolution. The degraded image is first restored and then recompressed. VRPSR optimizes the perceptual quality of the recompressed result. *right:* VRPSR saves more than 10% bitrate when evaluated with super-resolution methods such as Real-ESRGAN [33] and S3Diff [1], with codecs including H.264, H.265, and H.266.

# **Abstract**

Perceptual image super-resolution (SR) methods restore degraded images and produce sharp outputs. In practice, those outputs are usually recompressed for storage and transmission. Ignoring recompression is suboptimal as the downstream codec might add additional artifacts to restored images. However, jointly optimizing SR and recompression is challenging, as the codecs are not differentiable and vary in configuration. In this paper, we present Versatile Recompression-Aware Perceptual Super-Resolution (VRPSR), which makes existing perceptual SR aware of versatile compression. First, we formulate compression as conditional text-to-image generation and utilize a pre-trained diffusion model to build a generalizable codec simulator. Next, we propose a set of training techniques tailored for perceptual SR, including optimizing the simulator using perceptual targets and adopting slightly compressed images as the training target. Empirically, our VRPSR saves more

than 10% bitrate based on Real-ESRGAN and S3Diff under H.264/H.265/H.266 compression. Besides, our VRPSR facilitates joint optimization of the SR and post-processing model after recompression. Code and pretrained models are available at https://github.com/agus-official/VRPSR.

# 1. Introduction

Perceptual image super-resolution (SR) methods have shown great success in image restoration tasks [1, 32, 33], effectively generating sharp details from blurry inputs. However, a significant practical challenge remains: the restored images often need to be compressed again for storage and distribution. Without being aware of recompression, the fine details generated by SR methods might be turned into artifacts, leading to quality decay and a waste of bitrate.

<sup>\*</sup>These authors contributed equally to this work.  $\dagger$ To whom correspondence should be addressed.

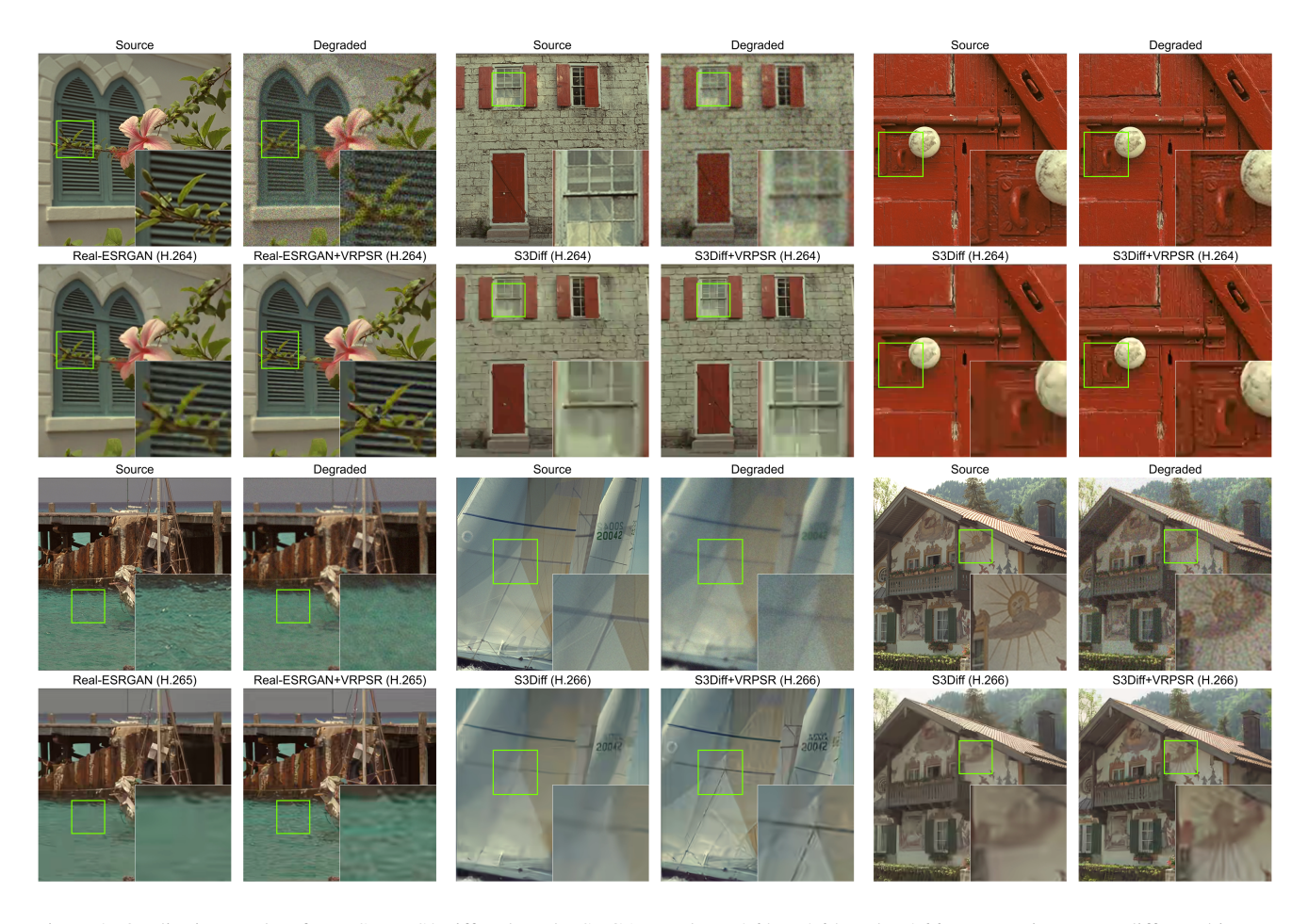


Figure 2. Qualitative results of VRPSR on S3Diff and Real-ESRGAN under H.264, H.265, and H.266 compression across different bitrates. It is shown that after compression, the SR methods with VRPSR produce significantly better visual results at the same bitrate.

Unfortunately, directly optimizing SR methods in conjunction with compression is not feasible, as image codecs are non-differentiable and vary substantially. While simple differentiable proxies [23, 37] exist for basic codecs such as JPEG [31], constructing accurate and generalizable differentiable proxies for modern codecs, such as H.265 [29] and H.266 [6], remains challenging. On the other hand, existing proxy-based differentiable codec simulators [18, 21] typically require separate training for each codec type and bitrate setting. A versatile codec proxy that generalizes across diverse conditions remains under-explored.

To address these challenges, we propose Versatile Recompression-Aware Perceptual Super-Resolution (VRPSR) to make existing perceptual image SR aware of recompression. First, we formulate image compression as a conditional text-to-image, which allows us to utilize existing pre-trained diffusion models. Next, we propose a set of training techniques tailored for perceptual SR, such as using a perceptual target to train the simulator and adopting a

slightly compressed image as supervision. Empirically, our VRPSR saves more than 10% bitrate on multiple SR algorithms and codecs. Furthermore, our accurate codec simulator enables the joint optimization of SR and post-processing after compression.

Our contributions can be summarized as follows:

- We propose Versatile Recompression-Aware Perceptual Super-Resolution (VRPSR), the first technique to make perceptual SR algorithms aware of recompression.
- We formulate image compression as a conditional text-toimage generation and utilize a pre-trained diffusion model for accurate and generalizable codec simulation.
- We introduce a set of training strategies tailored for perceptual SR, such as using a perceptual target for the simulator and training the SR model on slightly compressed images.
- Empirically, we demonstrate that VRPSR enhances the performance of multiple perceptual SR methods with a range of codecs for recompression.

 Furthermore, our accurate simulator enables the joint optimization of the SR model and an additional postprocessing module after recompression.

#### 2. Related Works

# 2.1. Perceptual Image Super-resolution

Perceptual image SR algorithms aim to achieve blind image restoration in real-world scenarios, where the degradation is unknown and training is typically conducted on synthetically generated data [33, 40]. Inspired by the perception-distortion trade-off theorem [5], early works in this area [33, 40] employed conditional Generative Adversarial Networks [10] to enhance perceptual quality. More recent approaches [1, 20, 25, 32, 34, 36, 39] adopt diffusion models [13, 28] to further improve generative capabilities. However, the task of recompression-aware perceptual SR remains under-explored.

# 2.2. Differentiable Image Codec Simulator

Differentiable image codec simulators aim to approximate the gradients of image codecs. These simulators generally fall into two categories: non-learning-based and learningbased. Non-learning-based simulators are typically designed for simple codecs such as JPEG [11, 14, 23, 37, 38] and H.264 [7], where non-differentiable components, such as quantization and mode decisions, are replaced with differentiable alternatives like the straight-through estimator [3] and Gumbel softmax [17, 22]. However, for more advanced codecs such as H.265 and H.266, constructing nonlearning-based simulators becomes prohibitively complex. Learning-based simulators use neural networks to approximate both the reconstruction and the bitrate produced by a real codec. For instance, Tian et al. [30] adopts DenseNet [16] to approximate the reconstruction of H.265. Subsequent works [18, 21] utilize hyperprior-based architectures [2] to approximate both rate and reconstruction for different codecs. However, these methods typically require a separate model for each codec type, whereas our VRPSR uses a single model for all codecs.

# 3. Versatile Recompression-Aware Perceptual Super-resolution

#### 3.1. Problem Formulation

Let X denote the clean image. We assume that the observed corrupted image  $\tilde{X}$  is generated via an unknown kernel  $p(\tilde{X}|X)$ . After obtaining  $\tilde{X}$ , the image is compressed by a codec  $f(\cdot;q)$  with parameter q, resulting in a compressed image  $\bar{X}$  with bitrate  $\bar{R}$ :

Corruption: 
$$\tilde{X} \sim p_C(\tilde{X}|X),$$
 Codec w/o SR:  $\bar{X}, \bar{R} = f(\tilde{X},q).$  (1)

To restore  $\tilde{X}$  and obtain a higher-quality image, we apply a perceptual SR model  $g_{\phi}(.)$ , producing a restored image X'. In a practical scenario, we need to keep the bitrate of the source image  $\tilde{X}$  and the processed image X' similar, as the network bandwidth is fixed. So when recompressing X', the codec parameter q' is adjusted such that the resulting bitrate  $\hat{R}$  matches  $\bar{R}$ . Specifically, we require a rate-preserving compression process:

$${\rm SR:}~X'=g_\phi(\tilde{X}),$$
 Codec w/ SR:  $\hat{X},\hat{R}=f(X',q'),$  select  $q'$  s.t.  $\hat{R}\approx\bar{R}.$  (2)

The optimization of the recompression-aware perceptual SR model parametrized by  $\phi$ , is typically formulated as a weighted combination of mean square error (MSE), LPIPS [43], and adversarial loss [5]:

$$\phi^* \leftarrow \arg\min_{\phi}, \Delta_S(\hat{X}, X), \text{ where } \Delta_S(\hat{X}, X)$$

$$= \mathcal{L}_{MSE}(\hat{X}, X) + \mathcal{L}_{LPIPS}(\hat{X}, X) + \mathcal{L}_{GAN}(\hat{X}). \tag{3}$$

A major challenge arises because the optimization target in Eq. 3 cannot be directly minimized using gradient descent, as the rate-preserving compression process described in Eq. 2 is not differentiable, and the codec type and parameter q can vary widely.

# 3.2. Image Codec Simulation as Text to Image

To optimize Eq. 3, we must simulate the rate-preserving image compression process described in Eq. 2 using a differentiable function, *i.e.*, computing  $d\hat{X}/dX'$ . Besides, it is essential to account for the diversity of codecs  $f(\cdot;q)$ . To address both challenges, we propose formulating codec simulation as a text-to-image problem to utilize a pre-trained diffusion model.

#### 3.2.1. Rate-Target Codec Simulation

Most existing codec simulators [7, 18, 21, 26, 30] directly approximate the gradient of the codec  $f(\cdot;q)$  by training a neural network  $f_{\theta}(\cdot,\cdot)$ , parameterized by  $\theta$ , to mimic the behavior of the actual codec for a given encoding parameter q. Both the bitrate  $\hat{R}$  and the reconstruction  $\hat{X}$  need to be learned. However, they cannot directly simulate the rate-preserving compression process in Eq. 2 as the selection of q' remains non-differentiable. On the other hand, we propose to directly approximate the output of the rate-preserving encoding process, with the bitrate as input. Formally, given a distortion metric  $\Delta_C(\cdot,\cdot)$ , the optimization target of our rate-target codec simulator is defined as:

$$\hat{X}' = f_{\theta}(X', \bar{R}),$$
 
$$\theta^* \leftarrow \arg\min_{\theta} \Delta_C(\hat{X}', \hat{X}), \text{ where } \hat{X} \text{ is from Eq. 2.} \quad (4)$$

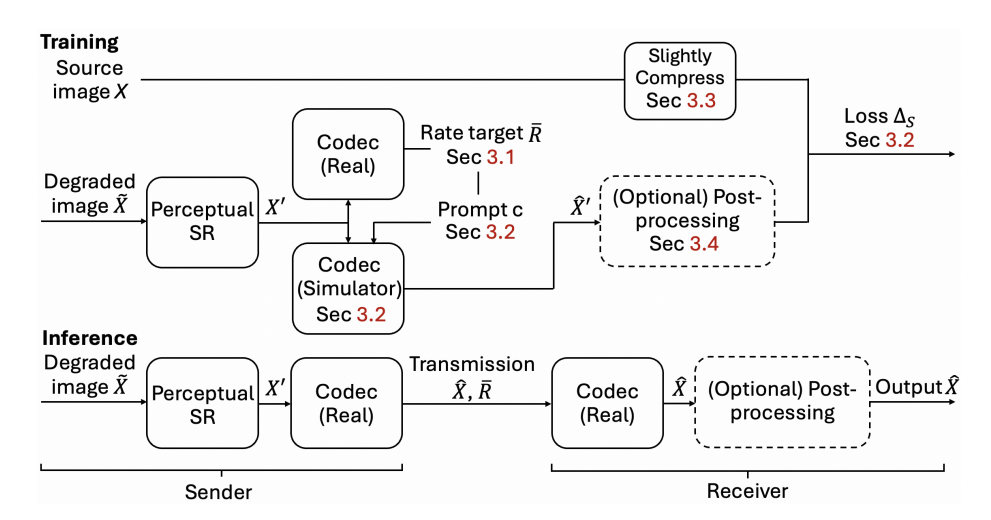


Figure 3. The training and inference pipeline of VRPSR. For training, we adopt a rate target codec simulator and use a slightly compressed image for supervision. For inference, the degraded image  $\tilde{X}$  is first restored by a perceptual super-resolution method to obtain X'. Then it is compressed by the encoder into  $\hat{X}$  with bitrate  $\bar{R}$ . Then, the compressed image is transmitted from the sender to the receiver. Then we either directly use image  $\hat{X}$  as the final output, or optionally include a post-processing module.

Table 1. Quantitative results on the Kodak dataset. Our VRPSR saves more than 10% bitrate on the perceptual metric.

			H.264 (x26	64)				H.265 (x26	55)		H.266 (vvenc)				
	bpp	PSNR	LPIPS	DISTS	FID	bpp	PSNR	LPIPS	DISTS	FID	bpp	PSNR	LPIPS	DISTS	FID
	0.11	26.01	0.467	0.277	146.63	0.15	26.70	0.471	0.254	148.83	0.14	27.38	0.425	0.227	99.54
Real-ESRGAN	0.16	26.85	0.403	0.242	102.90	0.21	27.31	0.418	0.225	100.13	0.18	27.59	0.403	0.214	80.57
Real-ESRGAN	0.25	27.30	0.365	0.220	82.59	0.28	27.62	0.386	0.208	78.77	0.23	27.72	0.387	0.205	71.64
	0.44	27.78	0.319	0.189	62.31	0.40	27.87	0.354	0.190	63.92	0.37	27.90	0.357	0.189	61.76
	0.11	25.79	0.450	0.264	137.07	0.15	26.22	0.455	0.238	132.42	0.14	27.13	0.409	0.213	86.62
Real-ESRGAN	0.16	26.64	0.388	0.230	90.19	0.21	26.99	0.400	0.212	85.40	0.18	27.39	0.385	0.202	76.30
	0.25	27.15	0.348	0.206	77.23	0.28	27.39	0.368	0.196	74.68	0.23	27.57	0.368	0.193	67.40
+VRPSR (Ours)	0.44	27.64	0.296	0.179	57.27	0.40	27.71	0.327	0.179	57.98	0.37	27.77	0.327	0.177	58.91
	BDBR	17.43%	-13.07%	-17.13%	-21.07%	BDBR	26.63%	-12.31%	-16.86%	-20.83%	BDBR	33.44%	-24.68%	-30.01%	-13.79%
	0.09	25.39	0.501	0.295	160.73	0.13	25.95	0.495	0.269	156.18	0.11	26.50	0.445	0.242	119.55
S3Diff	0.13	26.05	0.436	0.259	118.89	0.17	26.43	0.436	0.236	118.03	0.14	26.64	0.413	0.222	93.11
SSDIII	0.16	26.31	0.402	0.241	95.29	0.21	26.59	0.409	0.221	96.47	0.18	26.72	0.384	0.209	79.59
	0.28	26.61	0.343	0.205	66.78	0.30	26.76	0.353	0.194	69.61	0.23	26.78	0.361	0.194	66.47
	0.09	24.95	0.463	0.265	139.43	0.13	25.25	0.474	0.245	129.69	0.11	25.98	0.422	0.211	86.43
S3Diff	0.13	25.66	0.404	0.232	89.52	0.17	25.99	0.413	0.215	88.83	0.14	26.36	0.390	0.196	74.11
	0.16	26.02	0.375	0.217	78.91	0.21	26.26	0.385	0.200	75.51	0.18	26.56	0.367	0.186	63.58
+VRPSR (Ours)	0.28	26.49	0.323	0.186	58.53	0.30	26.64	0.342	0.180	56.67	0.23	26.68	0.346	0.175	54.25
	BDBR	27.05%	-19.40%	-29.05%	-27.50%	BDBR	35.24%	-12.02%	-21.76%	-22.70%	BDBR	53.67%	-16.21%	-38.31%	-29.54%

# 3.2.2. Codec Simulation as Text-to-Image Generation

To enhance the versatility of our simulator  $f_{\theta}(.)$  across various codec types, we propose to formulate the codec simulation as a conditional text-to-image task. For example, if the codec  $f(\cdot;q)$  is H.264 (x264) with a target bitrate 0.3 bits per pixel (bpp), the corresponding text prompt would be:

$$c = A \{ \text{libx264} \} \{ \text{0.3} \} \text{ bpp compressed image.}$$

Under this formulation, the rate-target codec simulator in Eq. 4 becomes a conditional text-to-image generation:

$$\hat{X}' = f_{\theta}(X', c). \tag{5}$$

This formulation allows the simulator in Eq. 5 to leverage powerful pre-trained text-to-image models, such as Stable

Diffusion [24], with additional image condition inputs X' as supported by models like ControlNet [41]. In practice, we implement  $f_{\theta}(.,.)$  with S3Diff [1], which is based on distilled Stable Diffusion [27].

# 3.2.3. Additional Codec Condition Embedding

In addition to including codec parameters in the prompt c, we inject them into SR backbones and the simulator via position embedding. More specifically, we treat the codec type as a one-hot vector, concatenate it with the target bpp, and transform them into an embedding vector similar to the temporal embedding of Stable Diffusion [24]. For the Real-ESRGAN backbone, we feed the embedding vector into residual blocks using AdaIN modulation [15]. For

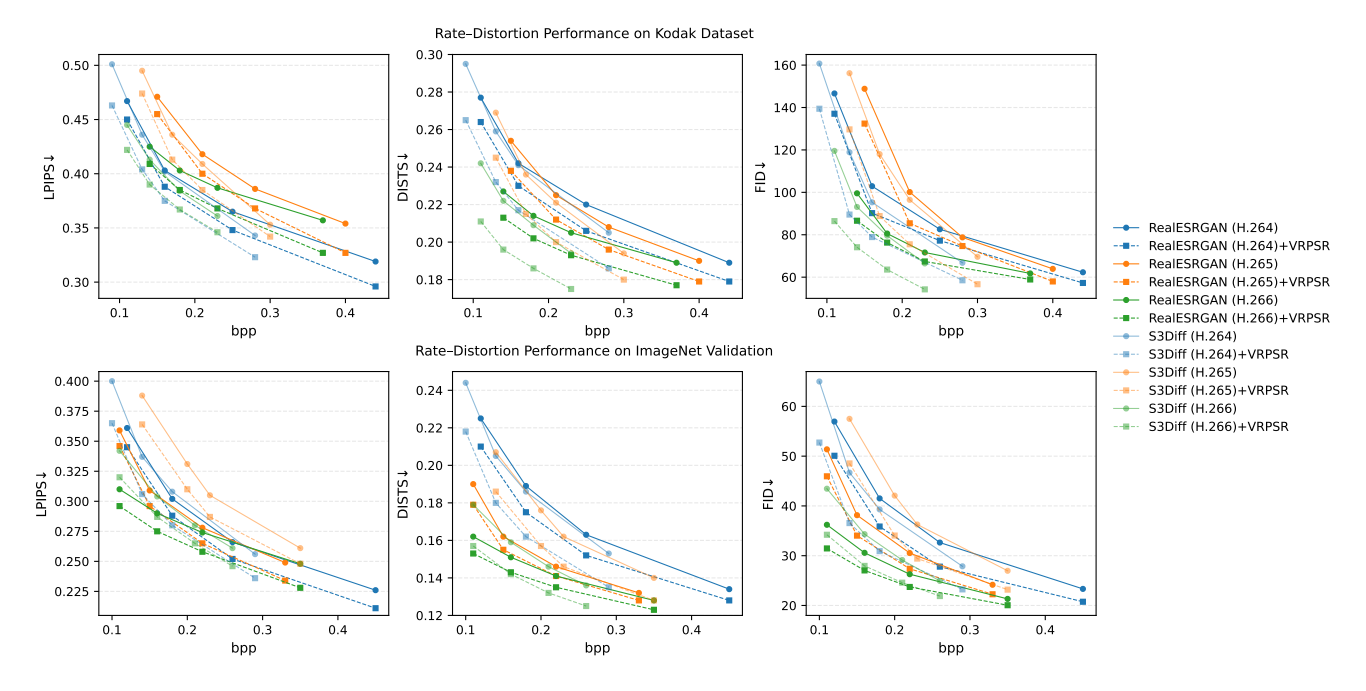


Figure 4. Rate-distortion performance on Kodak and ImageNet Validation dataset. Our VRPSR boosts the performance of RealESRGAN and S3Diff with multiple downstream codecs such as H.264, H.265, and H.266.

the S3Diff backbone, we add the embedding vector to the time embedding (see Appendix B for details). Empirically, we find that the additional embedding improves the performance of both the simulator and the final SR model.

# 3.3. Training Techniques for Perceptual SR

Empirically, we find that following previous simulators training [18, 30] that are designed for MSE-oriented SR is suboptimal for perceptual SR. Therefore, we propose several techniques tailored for training recompression-aware perceptual SR.

#### 3.3.1. Perceptual Training Target for the Simulator

Most existing approaches train codec proxies using MSE between the simulator output and the ground-truth codec output, even when the simulator is intended for perceptual applications [18, 30]. In contrast, we demonstrate that training the simulator with the perceptual target yields better results. Accordingly, we align the optimization target of the simulator in Eq. 4 with the target in SR training:

$$\Delta_C(\hat{X}', \hat{X}) = \Delta_S(\hat{X}', \hat{X}). \tag{6}$$

As shown in Tab. 3, optimizing with perceptual loss has minimal impact on PSNR but leads to significant improvements in perceptual quality metrics.

#### 3.3.2. Slightly Compressed Image for Supervision

By default, perceptual SR training is supervised against the clean image X. However, we empirically find that this leads

to unstable training and suboptimal performance, likely because the clean image is too far from the best image a codec can produce. Therefore, we propose to train the compression-aware SR model using a slightly compressed image. More specifically, we process X with our simulator using a configuration c' that compresses X slightly, where c''s bpp is set as the target quantization parameter q-10:

$$X_s = f_{\theta}(X, c'). \tag{7}$$

# 3.3.3. Two Stage Optimization

We adopt a two-stage optimization scheme for training the codec simulator and recompression-aware SR. First, the codec simulator is trained independently using the compressed outputs of ground-truth images X. Next, the SR parameter  $\phi(.)$  is updated iteratively with the simulator parameter  $\theta$  frozen. During SR updates, we use the output of SR X', rather than the ground-truth images, as input. Unlike prior works [18], we find that jointly updating the simulator and SR model is harmful to performance and stick to separate optimization.

# 3.3.4. No Straight-Through Estimator

Once the simulator output  $\hat{X}' = f_{\theta}(X',c)$  is obtained, the most straightforward strategy is to directly use  $\hat{X}'$  in place of the true codec output  $\hat{X}$  in Eq. 3. In contrast, many prior works [18, 21] adopt the straight-through estimator (STE) [3], claiming improved performance. STE is a training technique that replaces the simulator output  $\hat{X}'$  with true codec

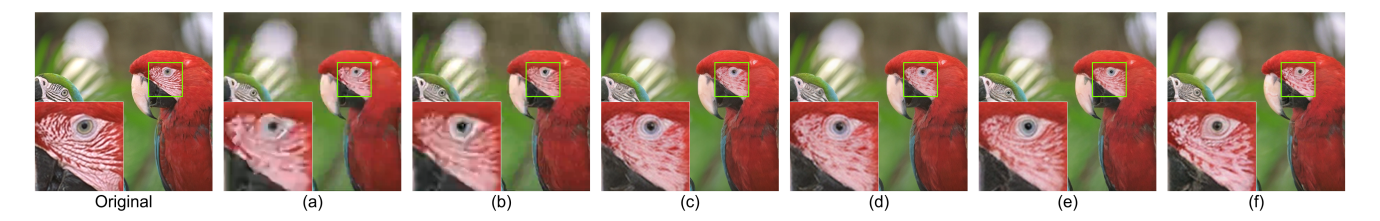


Figure 5. Qualitative results of optional post-processing. See definition of (a)-(f) in Table 2.

Table 2. Quantitative results of optional post-processing. Jointly training SR and post-processing brings the best result. Bold: Best.

ID	Perceptual SR	VRPSR	Post-processing	Optimization		S3	Diff + H.	264	
	r ereeptum Brt	, 111 511	r ost processing	оринидиион	bpp	PSNR	LPIPS	DISTS	FID
(a)	1	Х	Х	SR only	0.16	26.31	0.402	0.241	95.29
(b)	✓	✓	×	SR only	0.16	26.02	0.375	0.217	78.91
(c)	×	X	✓	Post only	0.16	26.09	0.275	0.157	52.08
(d)	✓	Х	✓	SR then Post	0.16	26.01	0.286	0.166	53.36
(e)	✓	✓	✓	SR then Post	0.16	25.81	0.274	0.157	52.81
(f)	✓	✓	✓	Joint	0.16	25.76	0.241	0.144	49.31

output  $\hat{X}$  during the forward pass, while preserving the gradient of the simulator during backpropagation. This can be implemented using a stop-gradient operator from the autograd package sg(.):

no STE: 
$$\hat{X}=\hat{X}',$$
 STE:  $\hat{X}_{\rm STE}=\hat{X}+\hat{X}'-{\rm sg}(\hat{X}').$  (8)

We conduct a comprehensive study on the impact of using STE. Our findings reveal that using the simulator output directly without STE yields better performance.

# 3.4. Optional Joint Post-Processing

Despite VRPSR improving the perceptual SR's performance with recompression, the overall performance of VRPSR is still bounded by the final codec. When the bitrate target is low, extremely heavy recompression still produces images with strong artifacts (see Appendix C for details). To tackle this challenge, we further propose an optional post-processing module after the recompression as shown in Figure 3. More specifically, we propose an additional post-processing network after the codec output  $\hat{X}$ , with prompt c as condition:

$$\hat{X}_{post} = h_{\phi}(\hat{X}, c). \tag{9}$$

With a differentiable codec simulator, the perceptual SR and post-processing module can be jointly optimized. Empirically, we show that such joint optimization leads to favourable results both quantitatively and qualitatively.

# 4. Experimental Results

# 4.1. Experimental Setup

For SR baselines, we select Real-ESRGAN [33] and **S3Diff** [1], which are two representative perceptual SR methods based on GANs and diffusion, respectively. All models are trained on the ImageNet [8] training split. For evaluation, we use the Kodak [19] and the ImageNet validation split. All images are resized and center-cropped to  $512 \times 512$ . We evaluate performance using the standard metrics for perceptual image SR: Peak Signal-to-Noise Ratio (PSNR), Learned Perceptual Image Patch Similarity (LPIPS) [42], Deep Image Structure and Texture Similarity (DISTS) [9], and Fréchet Inception Distance (FID) [12]. We also compute Structural Similarity (**SSIM**) [35] and report it in the supplementary material (Appendix C). To assess performance across varying bitrates, we additionally compute the Bjontegaard Bitrate (BDBR), a widely used metric for measuring average bitrate savings [4]. For simulator comparison, we include JPEG based simulator [11, 14] and **Hyper-prior** based simulators [18, 21], which are among the most commonly adopted in recent literature. For the downstream codec, we select three widely used compression standards of increasing complexity: H.264 (x264), H.265 (x265), and H.266 (vvenc). We exclude JPEG from our primary evaluation due to its simplicity and the availability of specialized simulators [23]. See Appendix A for more details.

#### 4.2. Results of VRPSR

In Table 1, Figure 2, and Figure 4, we show the effectiveness of VRPSR applied to both Real-ESRGAN and S3Diff on the Kodak and ImageNet datasets. Compared to base-

Table 3 Ablation stud	y on the design components of	four proposed simulator	Results are reported on the Kodak set.
Table 5. Adianon stud	y on the design components of	i oui proposcu simulator.	Results are reported on the Rodak set.

ID	Pre-train	Prompt	Embed	Output	Target	Simulator					S3Diff+H.264					
	(Sec 3.2.2)	(Sec 3.2.2)	(Sec 3.2.3)	(Sec 3.2.1)	(Sec 3.3.1)	PSNR	LPIPS	DISTS	FID	bpp	PSNR	LPIPS	DISTS	FID		
(a)	Х	✓	✓	$\hat{X}'$ , keep $\hat{R}' = \bar{R}$	Perceptual	26.35	0.374	0.213	117.09	0.10	25.58	0.498	0.285	151.12		
(b)	✓	<b>√</b> (no $\hat{R}'$ )	$\checkmark$ (no $\hat{R}'$ )	$\hat{X}', \hat{R}'$	Perceptual	28.67	0.168	0.116	61.22	0.10	25.66	0.479	0.282	150.41		
(c)	✓	×	×	$\hat{X}'$ , keep $\hat{R}' = \bar{R}$	Perceptual	28.85	0.209	0.164	89.98	0.10	25.61	0.482	0.284	154.30		
(d)	✓	✓	×	$\hat{X}'$ , keep $\hat{R}' = \bar{R}$	Perceptual	28.73	0.161	0.103	54.33	0.10	25.15	0.460	0.269	143.62		
(e)	✓	✓	1	$\hat{X}'$ , keep $\hat{R}' = \bar{R}$	MSE	30.93	0.192	0.167	92.31	0.10	25.42	0.461	0.274	165.82		
(f)	✓	✓	✓	$\hat{X}'$ , keep $\hat{R}' = \bar{R}$	Perceptual	29.43	0.157	0.101	50.13	0.10	24.95	0.459	0.264	130.99		

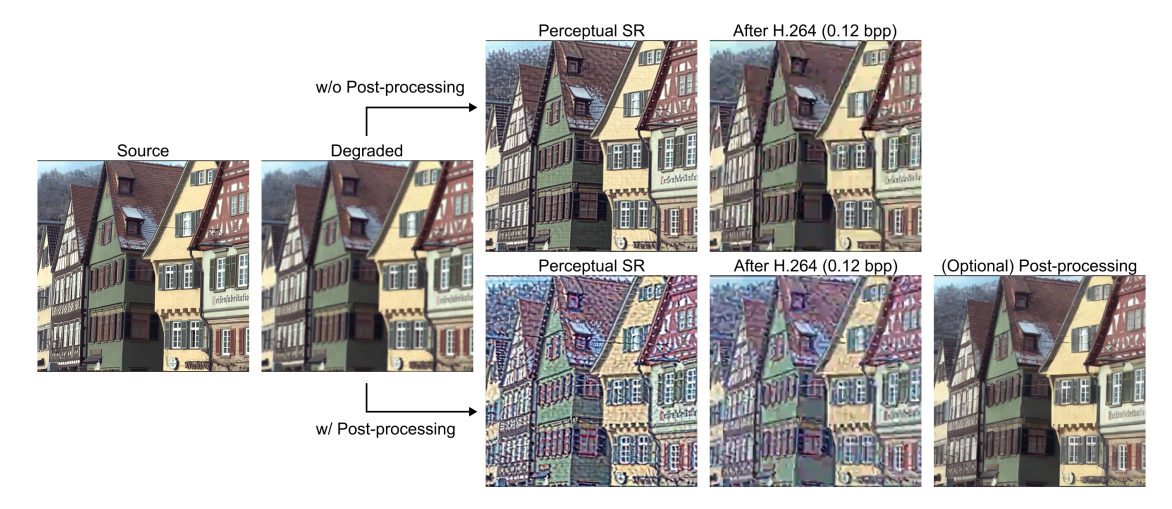


Figure 6. Qualitative results of VRPSR on S3Diff under H.264 recompression. The final output with the post-processing module effectively removes codec artifacts and restores perceptual details.

Table 4. Correlation between the performance of the simulator and final SR results. Despite the correlation between PSNR of the simulator and SR being weak, the correlation between perceptual metrics of the simulator and SR is strong.

	PSNR	LPIPS	DISTS	FID
$\overline{r^2}$ btw. Simulator and SR	0.105	0.690	0.490	0.435

line models trained without recompression-aware strategies, VRPSR achieves substantial bitrate savings—ranging from 10%-40%—when evaluated using perceptual metrics such as LPIPS, DISTS, and FID. These improvements are consistent across different codec types (H.264, H.265, and H.266) and a wide range of bitrates (from 0.09 to 0.45 bpp). Additional quantitative results on the ImageNet validation set are provided in the supplementary material (Table S1). As shown in Figure 2, the visual improvements introduced by VRPSR are also significant and clearly perceptible.

# 4.3. Results of VRPSR with Post-processing

Despite VRPSR successfully improving perceptual SR when facing recompression, its performance is still bounded by the codec, especially in the low bitrate regime. In that

case, our optional post-processing module can further boost the performance of VRPSR. As shown in Table 2, we compare several different ways to train post-processing. In Figure 5 and Table 2, we first confirm that the perceptual SR with VRPSR is much better than the perceptual SR without recompression awareness (Table 2 (a) vs (b)). Next, we show that training post-processing alone is better than SR alone (Table 2 (c) vs (b)), and training post-processing on top of perceptual SR is better than post-processing alone (Table 2 (d) (e) vs (c)). Finally, we show that joint training of post-processing and perceptual SR with a gradient estimated by VRPSR is the best (Table 2 (f) vs (d)(e)).

#### 4.4. Ablation Study on VRPSR Simulator

**Effectiveness of Simulator Component** In Tab. 3, we validate the effectiveness of various design components in our simulator. It is shown that using bitrate as input instead of output improves the performance of final SR (Table 3 (b) vs (f)). Besides, loading a pre-trained text-to-image diffusion model is also vital to performance (Table 3 (a) vs (f)). Further, including codec information as a prompt and embedding is beneficial (Table 3 (c) (d) vs (f)). And finally, using a perceptual target instead of an MSE target to train the simulator also improves the perceptual metric of the fi-

Table 5. Ablation of training strategies	(S3Diff + H.264)	). Results are re	ported on the Kodak set.

ID	STE	2 Stage Optimization	SR Embed	Versatile Model	Slightly Compressed Supervision		S3Diff + H.264						
	(Sec 3.3.4)	(Sec 3.3.3)	(Sec 3.2.3)	(Sec 3.2.2)	(Sec 3.3.2)	bpp	PSNR	LPIPS	DISTS	FID			
(a)	✓	✓	✓	/	Simulator	0.13	22.50	0.446	0.255	144.05			
(b)	×	×	✓	✓	Simulator	0.13	25.03	0.419	0.257	137.12			
(c)	×	✓	×	✓	Simulator	0.13	25.74	0.412	0.237	97.06			
(d)	×	✓	✓	×	Simulator	0.13	25.56	0.405	0.235	92.38			
(e)	×	✓	✓	✓	×	0.13	25.18	0.427	0.242	107.82			
(f)	×	✓	✓	✓	Real Codec	0.13	25.68	0.415	0.240	91.02			
(g)	X	✓	✓	✓	Simulator	0.13	25.66	0.404	0.232	89.52			

Table 6. Comparison with other simulators.

Simulator	S3Diff (H.264)											
	bpp	PSNR	LPIPS	DISTS	FID							
JPEG	0.13	25.98	0.436	0.255	125.92							
Hyperprior	0.13	26.22	0.445	0.257	117.49							
VRPSR (Ours)	0.13	25.66	0.404	0.232	89.52							

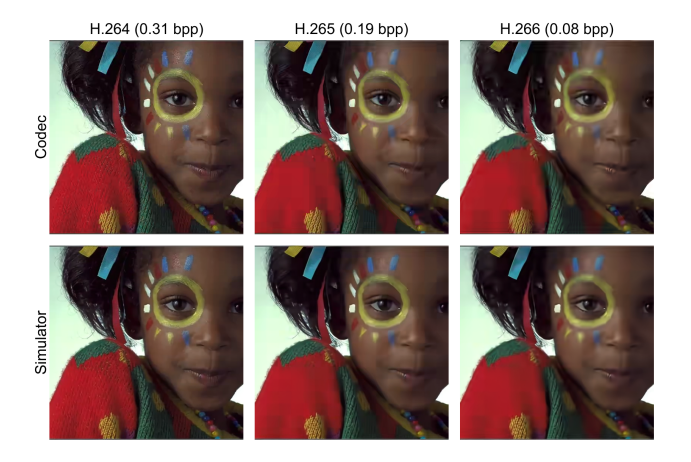


Figure 7. Qualitative results of the simulator under H.264, H.265, and H.266 compression.

nal SR (Table 3 (e) vs (f)).

Comparison to Other Simulators Furthermore, Table 6 shows that our simulator outperforms both JPEG-based and hyperprior-based simulators in terms of perceptual quality. As illustrated in Figure 7 and in the supplementary visualization in Figure S4, our simulator not only produces post-codec results with the best perceptual quality, but its simulated outputs are also the closest to the real codec outputs. This supports the intuition that a more accurate codec simulator leads to better recompression-aware SR models.

Relationship Between Simulator Performance and SR Performance Observing Table 3, an interesting trend is that the PSNR of the simulator does not have much impact on the PSNR of the final SR. However, the perceptual metrics (LPIPS, DISTS, and FID) of the simulator seem to be more related to the perceptual metrics of SR. In Table 4,

we quantify this observation by showing the  $r^2$  correlation of different metrics between the simulator and SR. In fact, the PSNR of the simulator and SR is only weakly correlated ( $r^2=0.105$ ). However, for LPIPS, DISTS, and FID, the correlation is much stronger ( $r^2\geq 0.4$ ). This coincides with the early works that use differentiable proxy JPEG for training and other codecs for inference [14]. As the target is PSNR/MSE, the accuracy of the simulator is not important. However, for the perceptual target, the accuracy of the simulator becomes important. And as shown in Figure 7, the VRPSR simulator is quite accurate and captures the characteristics of a compressed image.

## 4.5. Ablation Study on VRPSR Training Technique

In Table 5, we show the effectiveness of our proposed training techniques tailored for perceptual SR. More specifically, we show that the additional conditional embedding is beneficial to final performance (Table 5 (c) vs (g)). Besides, we show that adopting the slightly compressed supervision also improves the performance, and using a simulator to generate the compressed supervision is better than using the real codec (Table 5 (e)(f) vs (g)). On the other hand, using STE significantly harms the performance (Table 5 (a) vs (g)). Besides, using two-stage optimization and training the model on versatile conditions helps the performance (Table 5 (b)(d) vs (g)).

## 5. Conclusion & Discussion

We introduced VRPSR, the first recompression-aware perceptual image super-resolution method. Specifically, we construct a codec simulator that generalizes well to various codec conditions, utilizing a powerful pre-trained diffusion model. Besides, we propose a series of training techniques tailored for perceptual super-resolution, including using a slightly compressed image as supervision and using perceptual targets to train the simulator. Across Real-ESRGAN and S3Diff under H.264/H.265/H.266, VRPSR consistently improves perceptual quality at matched bitrates. Beyond preprocessing, our accurate codec simulator also enables joint training of an optional post-processing module.

In this paper, we limit the codec parameter to the codec

type and target bpp. In fact, our VRPSR is compatible with richer controls, such as encoding preset and rate control parameters. Besides, our VRPSR can also be used to construct a pure codec with clean input. We will leave those topics for future work.

#### References

- [1] Zhang Aiping, Yue Zongsheng, Pei Renjing, Ren Wenqi, and Cao Xiaochun. Degradation-guided one-step image super-resolution with diffusion priors. *arxiv*, 2024. 1, 3, 4, 6
- [2] Johannes Ballé, David Minnen, Saurabh Singh, Sung Jin Hwang, and Nick Johnston. Variational image compression with a scale hyperprior. arXiv preprint arXiv:1802.01436, 2018. 3
- [3] Yoshua Bengio, Nicholas Léonard, and Aaron Courville. Estimating or propagating gradients through stochastic neurons for conditional computation. arXiv preprint arXiv:1308.3432, 2013. 3, 5
- [4] Gisle Bjontegaard. Calculation of average psnr differences between rd-curves. *VCEG-M33*, 2001. 6
- [5] Yochai Blau and Tomer Michaeli. The perception-distortion tradeoff. In *Proceedings of the IEEE conference on computer vision and pattern recognition*, pages 6228–6237, 2018. 3
- [6] Benjamin Bross, Ye-Kui Wang, Yan Ye, Shan Liu, Jianle Chen, Gary J Sullivan, and Jens-Rainer Ohm. Overview of the versatile video coding (vvc) standard and its applications. *IEEE Transactions on Circuits and Systems for Video Tech*nology, 31(10):3736–3764, 2021. 2
- [7] Aaron Chadha and Yiannis Andreopoulos. Deep perceptual preprocessing for video coding. In *Proceedings of the IEEE/CVF Conference on Computer Vision and Pattern Recognition*, pages 14852–14861, 2021. 3
- [8] Jia Deng, Wei Dong, Richard Socher, Li-Jia Li, K. Li, and Li Fei-Fei. Imagenet: A large-scale hierarchical image database. 2009 IEEE Conference on Computer Vision and Pattern Recognition, pages 248–255, 2009. 6
- [9] Keyan Ding, Kede Ma, Shiqi Wang, and Eero P Simoncelli. Image quality assessment: Unifying structure and texture similarity. *IEEE transactions on pattern analysis and ma*chine intelligence, 44(5):2567–2581, 2020. 6
- [10] Ian Goodfellow, Jean Pouget-Abadie, Mehdi Mirza, Bing Xu, David Warde-Farley, Sherjil Ozair, Aaron Courville, and Yoshua Bengio. Generative adversarial networks. *Communications of the ACM*, 63(11):139–144, 2020. 3
- [11] Onur G Guleryuz, Philip A Chou, Berivan Isik, Hugues Hoppe, Danhang Tang, Ruofei Du, Jonathan Taylor, Philip Davidson, and Sean Fanello. Sandwiched compression: Repurposing standard codecs with neural network wrappers. arXiv preprint arXiv:2402.05887, 2024. 3, 6
- [12] Martin Heusel, Hubert Ramsauer, Thomas Unterthiner, Bernhard Nessler, and Sepp Hochreiter. Gans trained by a two time-scale update rule converge to a local nash equilibrium. In *Neural Information Processing Systems*, 2017. 6
- [13] Jonathan Ho, Ajay Jain, and Pieter Abbeel. Denoising diffusion probabilistic models. *Advances in neural information processing systems*, 33:6840–6851, 2020. 3

- [14] Yueyu Hu, Chenhao Zhang, Onur G. Guleryuz, Debargha Mukherjee, and Yao Wang. Standard compliant video coding using low complexity, switchable neural wrappers. In *International Conference on Information Photonics*, 2024. 3, 6, 8
- [15] Xun Huang and Serge J. Belongie. Arbitrary style transfer in real-time with adaptive instance normalization. 2017 IEEE International Conference on Computer Vision (ICCV), pages 1510–1519, 2017. 4
- [16] Forrest Iandola, Matt Moskewicz, Sergey Karayev, Ross Girshick, Trevor Darrell, and Kurt Keutzer. Densenet: Implementing efficient convnet descriptor pyramids. arXiv preprint arXiv:1404.1869, 2014. 3
- [17] Eric Jang, Shixiang Gu, and Ben Poole. Categorical reparameterization with gumbel-softmax. *arXiv preprint arXiv:1611.01144*, 2016. 3
- [18] Muhammad Umar Karim Khan, Aaron Chadha, Mohammad Ashraful Anam, and Yiannis Andreopoulos. Perceptual video compression with neural wrapping. In *Proceedings of the Computer Vision and Pattern Recognition Conference*, pages 17743–17754, 2025. 2, 3, 5, 6
- [19] Eastman Kodak. Kodak lossless true color image suite (photocd pcd0992). http://rok.us/graphics/kodak, 1993. 6
- [20] Haoying Li, Yifan Yang, Meng Chang, Shiqi Chen, Huajun Feng, Zhihai Xu, Qi Li, and Yueting Chen. Srdiff: Single image super-resolution with diffusion probabilistic models. *Neurocomputing*, 479:47–59, 2022. 3
- [21] Guo Lu, Xingtong Ge, Tianxiong Zhong, Qiang Hu, and Jing Geng. Preprocessing enhanced image compression for machine vision. *IEEE Transactions on Circuits and Systems for Video Technology*, 2024. 2, 3, 5, 6
- [22] Chris J Maddison, Andriy Mnih, and Yee Whye Teh. The concrete distribution: A continuous relaxation of discrete random variables. arXiv preprint arXiv:1611.00712, 2016.
- [23] Christoph Reich, Biplob Debnath, Deep Patel, and Srimat Chakradhar. Differentiable jpeg: The devil is in the details. In Proceedings of the IEEE/CVF Winter Conference on Applications of Computer Vision, pages 4126–4135, 2024. 2, 3,
- [24] Robin Rombach, Andreas Blattmann, Dominik Lorenz, Patrick Esser, and Björn Ommer. High-resolution image synthesis with latent diffusion models. In *Proceedings of* the IEEE/CVF conference on computer vision and pattern recognition, pages 10684–10695, 2022. 4
- [25] Chitwan Saharia, Jonathan Ho, William Chan, Tim Salimans, David J Fleet, and Mohammad Norouzi. Image super-resolution via iterative refinement. *IEEE transactions on pattern analysis and machine intelligence*, 45(4):4713–4726, 2022. 3
- [26] Amir Said, Manish Kumar Singh, and Reza Pourreza. Differentiable bit-rate estimation for neural-based video codec enhancement. In 2022 Picture Coding Symposium (PCS), pages 379–383. IEEE, 2022. 3
- [27] Axel Sauer, Dominik Lorenz, Andreas Blattmann, and Robin Rombach. Adversarial diffusion distillation. In *European*

- Conference on Computer Vision, pages 87-103. Springer, 2024. 4
- [28] Yang Song, Jascha Sohl-Dickstein, Diederik P Kingma, Abhishek Kumar, Stefano Ermon, and Ben Poole. Score-based generative modeling through stochastic differential equations. arXiv preprint arXiv:2011.13456, 2020. 3
- [29] Gary J Sullivan, Jens-Rainer Ohm, Woo-Jin Han, and Thomas Wiegand. Overview of the high efficiency video coding (hevc) standard. *IEEE Transactions on circuits and systems for video technology*, 22(12):1649–1668, 2012. 2
- [30] Yuan Tian, Guo Lu, Xiongkuo Min, Zhaohui Che, Guangtao Zhai, Guodong Guo, and Zhiyong Gao. Self-conditioned probabilistic learning of video rescaling. In *Proceedings of the IEEE/CVF international conference on computer vision*, pages 4490–4499, 2021. 3, 5
- [31] Gregory K Wallace. The jpeg still picture compression standard. *Communications of the ACM*, 34(4):30–44, 1991. 2
- [32] Jianyi Wang, Zongsheng Yue, Shangchen Zhou, Kelvin CK Chan, and Chen Change Loy. Exploiting diffusion prior for real-world image super-resolution. *International Journal of Computer Vision*, 132(12):5929–5949, 2024. 1, 3
- [33] Xintao Wang, Liangbin Xie, Chao Dong, and Ying Shan. Real-esrgan: Training real-world blind super-resolution with pure synthetic data. In *International Conference on Computer Vision Workshops (ICCVW)*, 2021. 1, 3, 6
- [34] Yufei Wang, Wenhan Yang, Xinyuan Chen, Yaohui Wang, Lanqing Guo, Lap-Pui Chau, Ziwei Liu, Yu Qiao, Alex C Kot, and Bihan Wen. Sinsr: diffusion-based image superresolution in a single step. In Proceedings of the IEEE/CVF conference on computer vision and pattern recognition, pages 25796–25805, 2024. 3
- [35] Zhou Wang, Alan C Bovik, Hamid R Sheikh, and Eero P Simoncelli. Image quality assessment: from error visibility to structural similarity. *IEEE transactions on image processing*, 13(4):600–612, 2004. 6
- [36] Rongyuan Wu, Tao Yang, Lingchen Sun, Zhengqiang Zhang, Shuai Li, and Lei Zhang. Seesr: Towards semantics-aware real-world image super-resolution. In *Proceedings of the IEEE/CVF conference on computer vision and pattern recognition*, pages 25456–25467, 2024. 3
- [37] Yazhou Xing, Zian Qian, and Qifeng Chen. Invertible image signal processing. In *Proceedings of the IEEE/CVF conference on computer vision and pattern recognition*, pages 6287–6296, 2021. 2, 3
- [38] Jinhai Yang, Mengxi Guo, Shijie Zhao, Junlin Li, and Li Zhang. Self-asymmetric invertible network for compression-aware image rescaling. In *Proceedings of the AAAI Conference on Artificial Intelligence*, pages 3155–3163, 2023. 3
- [39] Zongsheng Yue, Jianyi Wang, and Chen Change Loy. Resshift: Efficient diffusion model for image super-resolution by residual shifting. *Advances in Neural Information Processing Systems*, 36:13294–13307, 2023. 3
- [40] Kai Zhang, Jingyun Liang, Luc Van Gool, and Radu Timofte. Designing a practical degradation model for deep blind image super-resolution. In *Proceedings of the IEEE/CVF international conference on computer vision*, pages 4791–4800, 2021. 3

- [41] Lvmin Zhang, Anyi Rao, and Maneesh Agrawala. Adding conditional control to text-to-image diffusion models. In Proceedings of the IEEE/CVF international conference on computer vision, pages 3836–3847, 2023. 4
- [42] Richard Zhang, Phillip Isola, Alexei A. Efros, Eli Shechtman, and Oliver Wang. The unreasonable effectiveness of deep features as a perceptual metric. 2018 IEEE/CVF Conference on Computer Vision and Pattern Recognition, pages 586–595, 2018. 6
- [43] Richard Zhang, Phillip Isola, Alexei A Efros, Eli Shechtman, and Oliver Wang. The unreasonable effectiveness of deep features as a perceptual metric. In *Proceedings of the IEEE conference on computer vision and pattern recognition*, pages 586–595, 2018. 3

# **Versatile Recompression-Aware Perceptual Image Super-Resolution**

# Supplementary Material

# A. Implementation Details

## A.1. Training Details

**Hardware & Software.** All experiments run on  $8 \times NVIDIA$  A800-80GB GPUs (CUDA 12.2), Python 3.8.10, Diffusers 0.25.1, and Accelerate 1.0.1.

**Batching Strategy.** We set the effective global batch size to 64 by adjusting the per-GPU micro-batch size and the number of gradient accumulation steps accordingly. For example, a micro-batch size of 1 requires 8 accumulation steps per GPU, while a micro-batch size of 2 requires 4, and so on:

 $8 \text{ (GPUs)} \times \text{micro-batch} \times \text{accumulation} = 64.$ 

#### **Training Schedules.**

- **Simulator pre-training:** 60 000 global steps; 10 000 global steps (ablation).
- **S3Diff fine-tuning:** 20 000 global steps (main); 10 000 global steps (ablation).
- **Real-ESRGAN fine-tuning:** 40 000 global steps.

The learning rate during VRPSR fine-tuning is set to  $2\times 10^{-5}$  for both Real-ESRGAN and S3Diff. For Real-ESRGAN, we follow the official setting  $(1\times 10^{-4})$  during its pre-training phase before switching to the VRPSR regime.

**Optimizer.** We adopt AdamW with PyTorch defaults:  $\beta_1 = 0.9$ ,  $\beta_2 = 0.999$ , weight\_decay = 0.01, and  $\varepsilon = 10^{-8}$ .

**Learning-Rate Scheduler.** We use the scheduler provided by diffusers.get\_scheduler (linear warm-up  $\rightarrow cosine$  decay). We set warmup\_steps and max\_train\_steps to the exact global-step counts listed above for each stage, ensuring one complete cosine cycle per run.

**Loss Weights.** We follow S3Diff's convention and set  $\lambda_{\rm L2}=2.0,\ \lambda_{\rm LPIPS}=5.0,\ \lambda_{\rm GAN}=0.5$  throughout all VRPSR stages.

#### A.2. Traditional Codec Details

We compile x264 (H.264), x265 (H.265), and vvenc (VVC H.266) as shared libraries (.so) and invoke their C APIs from Python. Each RGB image is converted to YUV 4:2:0, encoded and decoded by the same library, and

the reconstruction is fed back as the reference for the next input. This ensures full bit-exact consistency with the official binaries while allowing in-process gradient-free calls.

- **H.264** / **x264** Based on the official x264<sup>1</sup> encoder in constant-quantization (CQP) mode, using fixed QP values to control the bitrate.
- **H.265 / x265** Based on the official x265<sup>2</sup> implementation with similar settings.
- **H.266 / VVC (vvenc)** Using the vvenc encoder<sup>3</sup>.

All three codecs operate in single-picture mode (no B frames) so that each encoded image can be evaluated independently.

#### **B. Network Architecture**

# **B.1. Synthetic Degradation**

We follow Real-ESRGAN to synthesize LR–HR pairs using a *high-order* degradation process.

First order applies a random degradation chain: blur  $\rightarrow$  resize  $\rightarrow$  noise  $\rightarrow$  JPEG, while the second order repeats the chain with different hyperparameters and applies a sinc filter either before or after JPEG compression to simulate sharpening and expand the degradation diversity.

Such a design has been shown to better match real-world degradations than a single stage.

#### **B.2.** Differentiable Codec Simulator

Our simulator is built on top of the official S3Diff codebase and reuses the codec-aware conditioning as the S3Diff backbone in Fig. S1. Concretely, the UNet and text encoder remain unchanged; we only add the 4-D codec prompt  $c=[c_1,c_2,c_3,\mathrm{bpp}]$  (Sec. 3.2.3), which is Fourier-embedded into a vector t and injected via FiLM-style affine parameters  $(\gamma,\beta)$  in each ResnetBlock2D, exactly as in the SR backbone.

Given a super-resolution image X' and prompt c, the simulator outputs a rate-matched reconstruction  $\hat{X}'$  that mimics the image produced by the real codec at bitrate  $\bar{R}$ . Training follows the same perceptual loss (LPIPS + GAN) as the downstream SR model.

# **B.3. Super-Resolution Backbones**

**Codec-aware conditioning (shared).** Both backbones are made codec-aware by the same 4-D prompt c =

https://code.videolan.org/videolan/x264/

<sup>2</sup>https://bitbucket.org/multicoreware/x265\_git/ src/master/

https://github.com/fraunhoferhhi/vvenc

<sup>4</sup>https://github.com/ArcticHare105/S3Diff

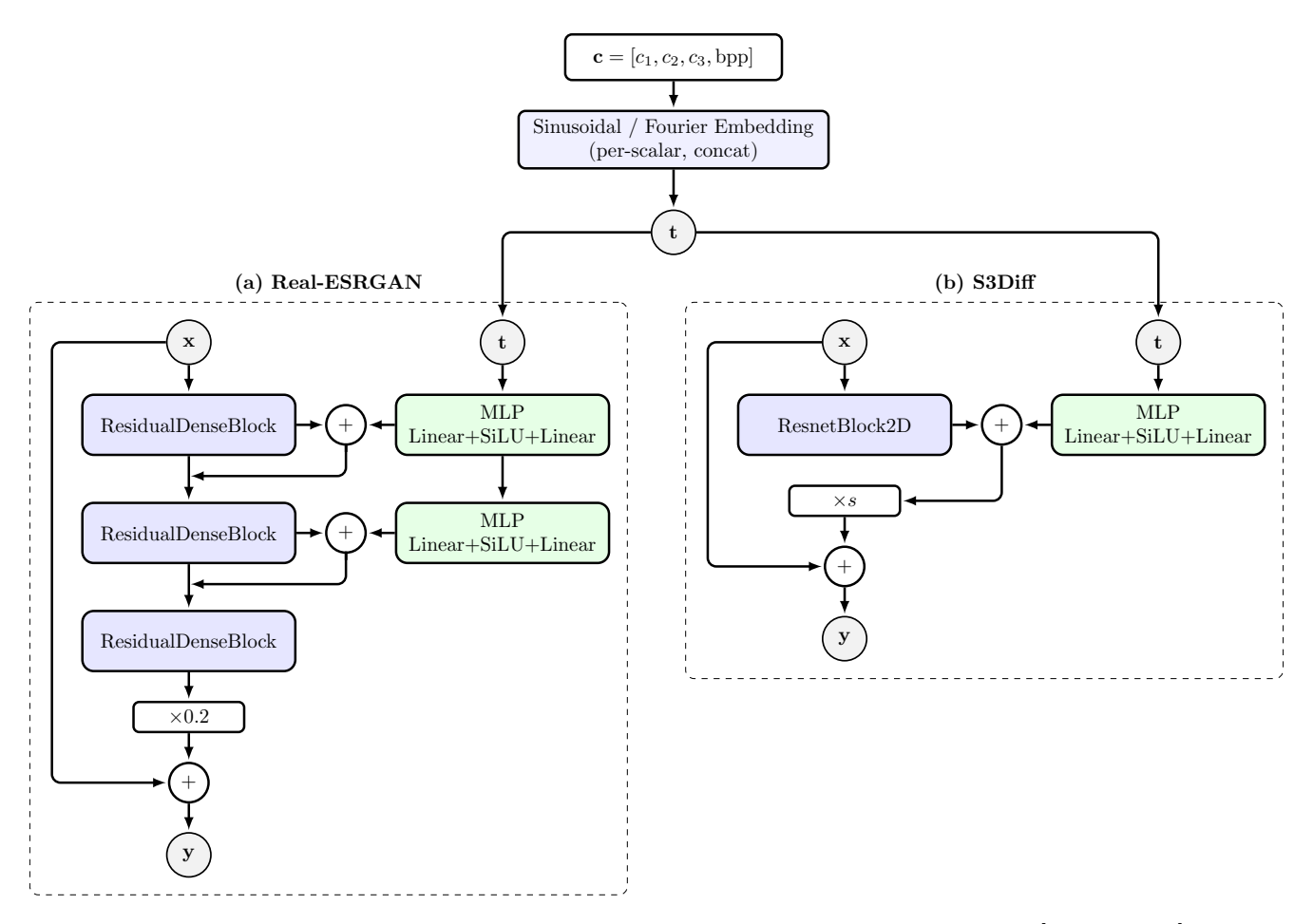


Figure S1. Unified codec-aware conditioning for Real-ESRGAN (left) and S3Diff (right). The 4-D prompt  $c = [c_1, c_2, c_3, \text{bpp}]$  is Fourier-embedded per scalar, concatenated, and then injected into the SR backbones as shown.

 $[c_1,c_2,c_3,\text{bpp}]$  (Sec. 3.2.3). As shown at the top of Fig. S1, each scalar is first mapped to sinusoidal/Fourier features and then concatenated into a single vector t. This shared embedding t is then fed into lightweight MLP heads attached to the SR backbones: for Real-ESRGAN, they produce per-channel bias terms that are additively injected into RRDB blocks, while for S3Diff, these heads produce FiLM-style affine parameters  $(\gamma,\beta)$ . All new MLP layers are zero-initialized in their last linear layer so that, at initialization, the conditioned model exactly matches the pretrained backbone.

Real-ESRGAN backbone. We start from the official Real-ESRGAN backbone and attach two tiny MLP heads per net that map t to channel-wise biases, which are added after the first two ResidualDenseBlocks. The third block and the outer residual path remain unchanged.

**S3Diff backbone.** We use the original S3Diff UNet and upgrade every ResnetBlock2D to a meta-conditioned

block that applies codec-aware FiLM parameters  $(\gamma, \beta)$  derived from the prompt c (Sec. 3.2.3). No other architectural or training changes are introduced.

# C. Additional Results

**Additional quantitative results.** Table S1 reports additional quantitative results on the ImageNet validation split, complementing the main-paper results on Kodak in Table 1. In addition, Figure S2 presents SSIM-based rate—distortion curves as a complementary full-reference metric to the perceptual RD results in Figure 4.

**Failure case and post-processing.** Under extremely heavy compression (very low bitrate), even VRPSR alone may fail to produce visually sharp results, and residual codec artifacts remain. However, as illustrated in Figure S3, the optional post-processing module introduced in Sec. 3.4 can largely remove these artifacts and recover sharper details, effectively mitigating this extreme failure case.

Table S1. Quantitative results on the ImageNet validation dataset.

			H.264 (x26	(4)				H.265 (x26	55)		H.266 (vvenc)				
	bpp	PSNR	LPIPS	DISTS	FID	bpp	PSNR	LPIPS	DISTS	FID	bpp	PSNR	LPIPS	DISTS	FID
	0.12	26.63	0.361	0.225	56.95	0.11	27.54	0.359	0.190	51.37	0.11	28.39	0.310	0.162	36.21
Real-ESRGAN	0.18	27.60	0.302	0.189	41.51	0.15	28.27	0.309	0.162	38.14	0.16	28.64	0.290	0.151	30.58
Real-ESKGAN	0.26	28.18	0.266	0.163	32.64	0.22	28.65	0.278	0.146	30.53	0.22	28.81	0.274	0.141	26.28
	0.45	28.78	0.226	0.134	23.33	0.33	28.95	0.249	0.132	24.16	0.35	29.01	0.248	0.128	21.32
	0.12	26.32	0.345	0.210	50.08	0.11	27.02	0.346	0.179	45.95	0.11	28.11	0.296	0.153	31.46
Real-ESRGAN	0.18	27.28	0.288	0.175	35.86	0.15	27.85	0.296	0.155	34.03	0.16	28.39	0.275	0.143	27.04
	0.26	27.89	0.252	0.152	27.80	0.22	28.31	0.265	0.141	27.37	0.22	28.58	0.258	0.135	23.72
+VRPSR (Ours)	0.45	28.50	0.211	0.128	20.75	0.33	28.64	0.234	0.128	22.25	0.35	28.75	0.228	0.123	20.05
	BDBR	20.83%	-12.60%	-16.17%	-18.07%	BDBR	14.88%	-10.30%	-10.82%	-12.53%	BDBR	39.16%	-19.81%	-17.52%	-17.44%
	0.10	25.84	0.400	0.244	65.00	0.14	26.60	0.388	0.207	57.50	0.11	27.17	0.342	0.179	43.46
S3Diff	0.14	26.63	0.337	0.205	46.69	0.20	27.12	0.331	0.176	42.07	0.16	27.38	0.304	0.159	34.33
SSDIII	0.18	26.92	0.308	0.186	39.30	0.23	27.28	0.305	0.162	36.27	0.21	27.48	0.280	0.146	29.13
	0.29	27.29	0.256	0.153	27.87	0.35	27.46	0.261	0.140	26.97	0.26	27.52	0.261	0.136	24.93
	0.10	25.40	0.365	0.218	52.73	0.14	26.04	0.364	0.186	48.54	0.11	26.79	0.320	0.157	34.21
S3Diff	0.14	26.26	0.306	0.180	36.55	0.20	26.76	0.310	0.157	34.05	0.16	27.16	0.287	0.142	27.95
+VRPSR (Ours)	0.18	26.60	0.280	0.162	30.91	0.23	27.02	0.287	0.146	29.42	0.21	27.32	0.265	0.132	24.58
+vKr3K (Ours)	0.29	27.07	0.236	0.135	23.23	0.35	27.35	0.248	0.128	23.18	0.26	27.41	0.246	0.125	21.89
	BDBR	24.01%	-20.13%	-25.07%	-24.48%	BDBR	27.23%	-12.53%	-20.67%	-19.49%	BDBR	42.02%	-15.84%	-30.08%	-27.45%

#### Rate-Distortion (SSIM vs bpp) on Kodak and ImageNet Validation

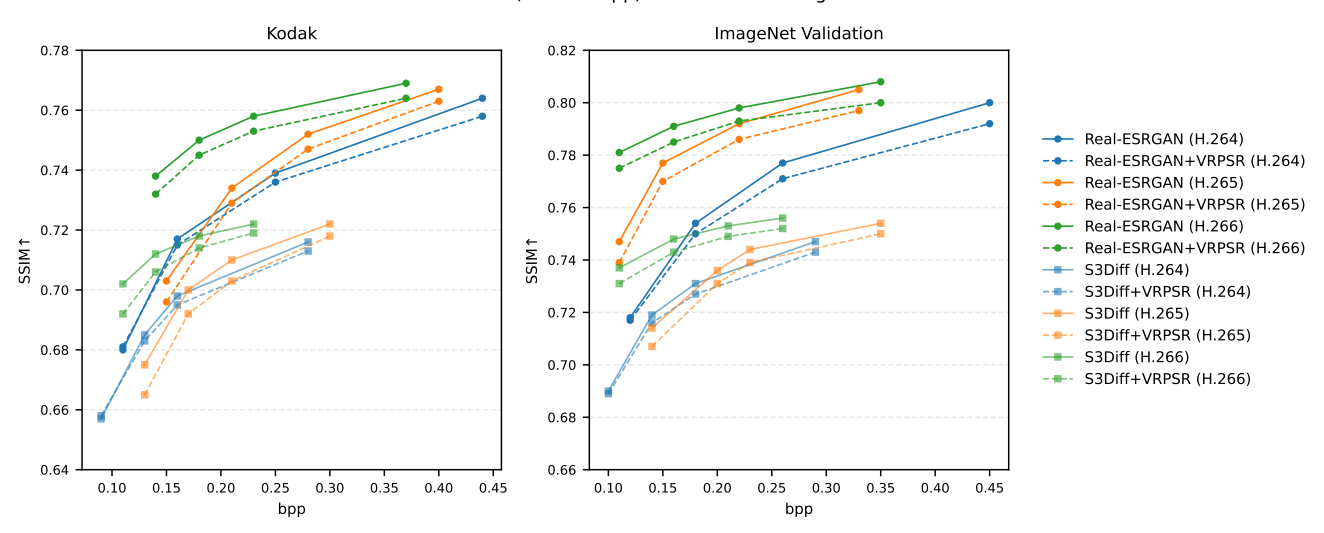


Figure S2. SSIM-based rate-distortion performance on the Kodak and ImageNet validation datasets. As a complementary full-reference metric to the perceptual curves in Figure 4, SSIM shows that VRPSR maintains competitive distortion while improving perceptual quality at matched bitrates.

**Simulator comparison.** In Figure S4, we visualize the setups corresponding to Table 6.

#### C.1. Statistical Analysis on Kodak and ImageNet

To complement the aggregate rate—distortion results in Tables 1 and 6, we report per-image statistics and simple significance tests on both the Kodak and ImageNet validation datasets. For each codec and bitrate setting, we compute PSNR, LPIPS, DISTS, and SSIM for every image and summarize the results as  $mean \pm standard\ deviation$ . We additionally perform two-sided paired t-tests between each baseline SR model and its VRPSR-enhanced counterpart

under the same codec and bitrate, using the per-image metrics.

Table S2 reports per-image statistics on Kodak (24 images) for Real-ESRGAN and S3Diff under H.264, H.265, and H.266. Table S3 shows the corresponding results on the ImageNet validation subset (1,000 images). Across almost all codec/bitrate configurations, VRPSR consistently improves the perceptual metrics (LPIPS, DISTS) at comparable bitrates, while PSNR and SSIM changes remain small. This behavior aligns with the perception—distortion trade-off: VRPSR shifts the operating point toward better perceptual quality with only minor fidelity changes. The

paired t-tests yield extremely small p-values for LPIPS and DISTS in nearly all settings (frequently well below  $10^{-3}$ , and in some ImageNet configurations numerically approaching the machine-precision floor, e.g.,  $< 10^{-300}$ ), indicating that the observed perceptual gains are statistically significant rather than arising from random variation. In contrast, the p-values for PSNR and SSIM are frequently much larger, confirming that the small average differences in these distortion-oriented metrics are less systematic. The trends on ImageNet largely mirror those on Kodak, suggesting that VRPSR generalizes well from small canonical test sets to more diverse, large-scale natural image distributions.

#### C.2. Generalization to Unseen Codec Parameter

In the main text, VRPSR is trained and evaluated with codecs operated in constant-quantization-parameter (CQP) mode. For each bpp, we select a QP to achieve it. To test the robustness of our VRPSR to unseen codec mode, we test our model with CRF rate control, which has never appeared during training.

Concretely, we use H.264 (x264) with four CRF values (26, 28, 32, 36), which correspond to average bitrates of roughly 0.10–0.35 bpp on Kodak (see Table S4). During inference, we measure the resulting bpp for each image and feed this measured bpp into VRPSR as the rate target, without any retraining or modification of the model. Table S4 reports the performance of S3Diff and S3Diff+VRPSR at the resulting average bitrates on Kodak, together with a BDBR summary over the four CRF points. This experiment complements the CQP-based results in the main paper and shows that VRPSR generalizes well to unseen codec parameters, consistently improving perceptual metrics (LPIPS, DISTS, FID) while maintaining comparable PSNR.

# D. Reproducibility Statement

For the experiments, we used publicly accessible datasets. Additional implementation details are provided in the appendix. Moreover, we include the source code for reproducing the experimental results in the supplementary material and will make it publicly available.



Figure S3. Failure case of VRPSR under extremely heavy compression and its mitigation by the optional post-processing module.



Figure S4. Qualitative comparison corresponding to Table 6. Each column shows a super-resolution model trained with a different simulator setting: (1) finetuned SR without an explicit codec simulator, (2) SR trained with a JPEG-based simulator, (3) SR trained with a hyperprior-based simulator, and (4) our VRPSR. Rows correspond to: (1) the SR output before compression, (2) the output after passing through the corresponding simulator, and (3) the output after the real codec. Our VRPSR achieves the best final post-codec quality, and its simulated outputs most closely match the real codec outputs, supporting the conclusion that a more accurate simulator leads to better SR models.

Table S2. Per-image statistics on the Kodak dataset under H.264, H.265, and H.266.

				Finet	une SR	VRPSR (Ours)					p-value (paired $t$ -test)				
Method	Codec	bpp	PSNR	LPIPS	DISTS	SSIM	PSNR	LPIPS	DISTS	SSIM	PSNR	LPIPS	DISTS	SSIM	
		0.11	$26.01 \pm 2.43$	$0.468 \pm 0.100$	$0.278 \pm 0.034$	$0.681 \pm 0.111$	$25.80 \pm 2.46$	$0.451 \pm 0.094$	$0.264 \pm 0.030$	$0.681 \pm 0.110$	3.00e-05	1.52e-04	1.93e-05	7.02e-01	
	H.264	0.16	$26.86 \pm 2.52$	$0.403 \pm 0.100$	$0.243 \pm 0.036$	$0.717 \pm 0.103$	$26.65 \pm 2.50$	$0.388 \pm 0.095$	$0.231 \pm 0.032$	$0.715 \pm 0.102$	1.30e-05	2.33e-04	1.87e-05	1.64e-01	
	H.204	0.25	$27.30 \pm 2.48$	$0.365 \pm 0.095$	$0.221 \pm 0.035$	$0.739 \pm 0.095$	$27.16 \pm 2.49$	$0.348 \pm 0.093$	$0.207 \pm 0.034$	$0.737 \pm 0.095$	3.86e-05	4.33e-06	5.24e-09	3.11e-02	
		0.44	$27.78 \pm 2.46$	$0.320\pm0.089$	$0.189 \pm 0.031$	$0.764\pm0.088$	$27.64 \pm 2.44$	$0.296 \pm 0.083$	$0.180\pm0.029$	$0.759 \pm 0.087$	6.03e-05	1.27e-07	2.52e-05	4.98e-05	
		0.15	$26.71 \pm 2.41$	$0.472\pm0.119$	$0.255 \pm 0.038$	$0.704\pm0.104$	$26.23 \pm 2.28$	$0.456\pm0.117$	$0.238\pm0.039$	$0.696\pm0.101$	1.35e-09	1.65e-06	1.23e-09	8.00e-07	
Real-ESRGAN	H.265	0.21	$27.32 \pm 2.46$	$0.419 \pm 0.116$	$0.225 \pm 0.037$	$0.734 \pm 0.097$	$27.00 \pm 2.37$	$0.400 \pm 0.116$	$0.212 \pm 0.037$	$0.730 \pm 0.095$	1.64e-06	5.02e-05	3.14e-07	6.12e-04	
	11.203	0.28	$27.63 \pm 2.45$	$0.386 \pm 0.111$	$0.208 \pm 0.036$	$0.753 \pm 0.092$	$27.40 \pm 2.39$	$0.368 \pm 0.114$	$0.196 \pm 0.036$	$0.748 \pm 0.091$	3.43e-05	4.26e-06	5.86e-08	1.90e-06	
		0.40	$27.87 \pm 2.44$	$0.354\pm0.105$	$0.191 \pm 0.035$	$0.768 \pm 0.087$	$27.71 \pm 2.40$	$0.328\pm0.102$	$0.179 \pm 0.033$	$0.763 \pm 0.086$	1.59e-04	1.48e-07	1.39e-09	1.61e-04	
		0.14	$27.39 \pm 2.51$	$0.426\pm0.115$	$0.227\pm0.036$	$0.738\pm0.096$	$27.14 \pm 2.45$	$0.409\pm0.112$	$0.214\pm0.035$	$0.733\pm0.095$	6.24e-07	4.38e-05	9.90e-09	6.21e-05	
	H.266	0.18	$27.60 \pm 2.50$	$0.403 \pm 0.114$	$0.215 \pm 0.038$	$0.751 \pm 0.093$	$27.39 \pm 2.46$	$0.386 \pm 0.112$	$0.202 \pm 0.037$	$0.745 \pm 0.093$	7.82e-07	9.16e-05	7.60e-08	4.38e-05	
		0.23	$27.73 \pm 2.51$	$0.387 \pm 0.113$	$0.206 \pm 0.039$	$0.758 \pm 0.091$	$27.57 \pm 2.47$	$0.368 \pm 0.112$	$0.194 \pm 0.035$	$0.754 \pm 0.090$	1.80e-05	5.84e-06	1.34e-06	5.68e-05	
		0.37	$27.90 \pm 2.48$	$0.358 \pm 0.108$	$0.190 \pm 0.037$	$0.770 \pm 0.087$	$27.78 \pm 2.45$	$0.328 \pm 0.103$	$0.178 \pm 0.034$	$0.764 \pm 0.086$	5.42e-05	8.99e-08	7.19e-06	6.91e-06	
		0.09	$25.39 \pm 2.45$	$0.502\pm0.106$	$0.296\pm0.031$	$0.657\pm0.122$	$24.96 \pm 2.51$	$0.464\pm0.095$	$0.265\pm0.029$	$0.658\pm0.120$	1.51e-08	9.36e-07	1.59e-11	4.48e-01	
	H.264	0.13	$26.06 \pm 2.51$	$0.437 \pm 0.104$	$0.259 \pm 0.034$	$0.686 \pm 0.115$	$25.67 \pm 2.50$	$0.404 \pm 0.094$	$0.232 \pm 0.031$	$0.683 \pm 0.114$	5.16e-07	1.07e-08	6.26e-11	2.03e-02	
	11.204	0.16	$26.31 \pm 2.52$	$0.403 \pm 0.103$	$0.241 \pm 0.037$	$0.699 \pm 0.111$	$26.03 \pm 2.55$	$0.375 \pm 0.095$	$0.217 \pm 0.033$	$0.696 \pm 0.113$	1.16e-05	4.71e-10	9.33e-11	7.55e-03	
		0.28	$26.62 \pm 2.51$	$0.343 \pm 0.096$	$0.205 \pm 0.035$	$0.716 \pm 0.106$	$26.49 \pm 2.57$	$0.323 \pm 0.086$	$0.186 \pm 0.030$	$0.713 \pm 0.106$	4.35e-03	2.36e-06	2.62e-09	5.54e-03	
		0.13	$25.96 \pm 2.36$	$0.496\pm0.116$	$0.269\pm0.036$	$0.676\pm0.111$	$25.25 \pm 2.28$	$0.475\pm0.115$	$0.245\pm0.037$	$0.665\pm0.111$	1.82e-11	9.33e-05	1.72e-10	1.44e-06	
S3Diff	H.265	0.17	$26.43 \pm 2.42$	$0.437 \pm 0.121$	$0.236 \pm 0.039$	$0.701 \pm 0.107$	$25.99 \pm 2.37$	$0.414 \pm 0.114$	$0.215 \pm 0.037$	$0.693 \pm 0.107$	6.70e-08	4.77e-05	1.88e-09	9.29e-06	
	11.203	0.21	$26.59 \pm 2.43$	$0.409 \pm 0.117$	$0.222 \pm 0.037$	$0.710 \pm 0.105$	$26.26 \pm 2.41$	$0.385 \pm 0.111$	$0.200 \pm 0.036$	$0.704 \pm 0.105$	1.92e-06	1.52e-06	3.61e-10	1.02e-06	
		0.30	$26.77 \pm 2.44$	$0.354 \pm 0.106$	$0.194 \pm 0.035$	$0.723 \pm 0.101$	$26.64 \pm 2.46$	$0.342 \pm 0.101$	$0.180 \pm 0.031$	$0.718 \pm 0.102$	2.88e-03	5.32e-03	8.25e-08	1.91e-04	
		0.11	$26.50 \pm 2.49$	$0.446\pm0.118$	$0.243 \pm 0.034$	$0.702\pm0.108$	$25.98 \pm 2.45$	$0.423\pm0.115$	$0.211\pm0.030$	$0.692\pm0.107$	3.55e-06	9.40e-04	6.34e-11	2.82e-04	
	H.266	0.14	$26.64 \pm 2.48$	$0.413 \pm 0.118$	$0.223 \pm 0.037$	$0.712 \pm 0.105$	$26.37 \pm 2.47$	$0.390 \pm 0.111$	$0.197 \pm 0.033$	$0.706 \pm 0.104$	7.86e-06	5.93e-04	8.86e-10	5.57e-04	
	11.200	0.18	$26.73 \pm 2.48$	$0.385 \pm 0.114$	$0.209 \pm 0.038$	$0.718 \pm 0.103$	$26.57 \pm 2.49$	$0.367 \pm 0.108$	$0.186 \pm 0.035$	$0.714 \pm 0.102$	3.88e-05	2.25e-03	1.72e-08	2.85e-04	
		0.23	$26.78 \pm 2.47$	$0.362 \pm 0.115$	$0.195 \pm 0.039$	$0.723 \pm 0.102$	$26.69 \pm 2.50$	$0.346 \pm 0.110$	$0.175 \pm 0.033$	$0.719 \pm 0.102$	4.01e-03	1.77e-03	1.37e-08	4.60e-04	

Table S3. Per-image statistics on the ImageNet Validation dataset under H.264, H.265, and H.266.

				Finet	une SR			VRPS	R (Ours)			p-value (pa	ired t-test)	
Method	Codec	bpp	PSNR	LPIPS	DISTS	SSIM	PSNR	LPIPS	DISTS	SSIM	PSNR	LPIPS	DISTS	SSIM
		0.12	$26.64 \pm 3.55$	$0.362 \pm 0.123$	$0.225 \pm 0.037$	$0.719 \pm 0.142$	$26.33 \pm 3.46$	$0.345 \pm 0.123$	$0.210 \pm 0.035$	$0.717 \pm 0.143$	1.13e-172	1.07e-139	1.07e-227	1.82e-11
	H.264	0.18	$27.61 \pm 3.76$	$0.302 \pm 0.120$	$0.189 \pm 0.039$	$0.755 \pm 0.132$	$27.28 \pm 3.64$	$0.289 \pm 0.120$	$0.175 \pm 0.036$	$0.750 \pm 0.134$	3.81e-209	4.54e-141	5.32e-196	1.20e-82
	H.204	0.26	$28.19 \pm 3.89$	$0.266 \pm 0.117$	$0.164 \pm 0.039$	$0.777 \pm 0.126$	$27.90 \pm 3.79$	$0.253 \pm 0.117$	$0.153 \pm 0.038$	$0.771 \pm 0.128$	8.71e-202	8.56e-153	3.99e-161	2.46e-122
		0.45	$28.79 \pm 4.05$	$0.226\pm0.113$	$0.135\pm0.039$	$0.800\pm0.120$	$28.51 \pm 3.97$	$0.211\pm0.110$	$0.128\pm0.039$	$0.792\pm0.122$	3.35e-181	1.69e-144	1.68e-93	3.87e-166
		0.11	$27.55 \pm 3.64$	$0.359\pm0.138$	$0.191 \pm 0.042$	$0.748\pm0.133$	$27.02 \pm 3.38$	$0.346\pm0.144$	$0.180\pm0.041$	$0.740\pm0.134$	2.43e-186	8.23e-62	1.21e-132	7.06e-125
Real-ESRGAN	H.265	0.15	$28.28 \pm 3.84$	$0.309 \pm 0.134$	$0.163 \pm 0.041$	$0.777 \pm 0.126$	$27.86 \pm 3.62$	$0.297 \pm 0.138$	$0.155 \pm 0.041$	$0.770 \pm 0.127$	4.76e-151	5.84e-76	9.63e-89	3.33e-139
	11.203	0.22	$28.66 \pm 3.96$	$0.279 \pm 0.131$	$0.147 \pm 0.041$	$0.793 \pm 0.122$	$28.31 \pm 3.78$	$0.266 \pm 0.132$	$0.141 \pm 0.040$	$0.786 \pm 0.123$	8.27e-141	8.06e-89	1.09e-57	2.09e-139
		0.33	$28.95 \pm 4.08$	$0.250 \pm 0.125$	$0.132 \pm 0.040$	$0.805 \pm 0.119$	$28.65 \pm 3.97$	$0.234 \pm 0.124$	$0.129 \pm 0.040$	$0.797 \pm 0.121$	2.92e-151	3.03e-106	1.30e-34	2.94e-144
		0.11	$28.40 \pm 3.99$	$0.311 \pm 0.133$	$0.162 \pm 0.040$	$0.781\pm0.126$	$28.12 \pm 3.89$	$0.296 \pm 0.133$	$0.153 \pm 0.039$	$0.775 \pm 0.128$	4.93e-164	1.64e-111	3.22e-117	5.12e-114
	H.266	0.16	$28.65 \pm 4.05$	$0.290 \pm 0.129$	$0.151 \pm 0.040$	$0.792 \pm 0.123$	$28.40 \pm 3.95$	$0.276 \pm 0.129$	$0.143 \pm 0.040$	$0.785 \pm 0.125$	1.06e-145	1.89e-133	2.98e-120	1.68e-127
	11.200	0.22	$28.82 \pm 4.09$	$0.274 \pm 0.127$	$0.142 \pm 0.040$	$0.799 \pm 0.121$	$28.58 \pm 3.99$	$0.259 \pm 0.125$	$0.136 \pm 0.040$	$0.793 \pm 0.122$	5.09e-136	1.17e-131	1.88e-83	1.68e-138
		0.35	$29.01 \pm 4.14$	$0.249 \pm 0.123$	$0.129 \pm 0.040$	$0.808\pm0.119$	$28.76 \pm 4.06$	$0.228 \pm 0.117$	$0.124 \pm 0.040$	$0.800\pm0.120$	4.62e-157	2.05e-154	1.75e-63	1.02e-175
		0.10	$25.84 \pm 3.43$	$0.400\pm0.126$	$0.244\pm0.036$	$0.690\pm0.153$	$25.41 \pm 3.39$	$0.365 \pm 0.122$	$0.218\pm0.036$	$0.689\pm0.152$	5.14e-226	1.82e-254	<1e-300	4.68e-02
	H.264	0.14	$26.63 \pm 3.66$	$0.337 \pm 0.123$	$0.206 \pm 0.037$	$0.720 \pm 0.147$	$26.26 \pm 3.61$	$0.307 \pm 0.117$	$0.180 \pm 0.034$	$0.716 \pm 0.148$	5.60e-220	8.73e-252	<1e-300	3.24e-46
	11.204	0.18	$26.92 \pm 3.76$	$0.309 \pm 0.120$	$0.187 \pm 0.038$	$0.731 \pm 0.146$	$26.61 \pm 3.71$	$0.280 \pm 0.114$	$0.163 \pm 0.034$	$0.727 \pm 0.146$	6.60e-180	1.43e-243	1.48e-309	5.70e-64
		0.29	$27.29 \pm 3.91$	$0.257\pm0.112$	$0.153 \pm 0.037$	$0.747\pm0.143$	$27.08 \pm 3.85$	$0.236 \pm 0.106$	$0.135\pm0.034$	$0.743\pm0.144$	2.90e-98	3.69e-171	4.95e-250	5.48e-81
		0.14	$26.61 \pm 3.56$	$0.389 \pm 0.139$	$0.208 \pm 0.042$	$0.714 \pm 0.148$	$26.04 \pm 3.39$	$0.364 \pm 0.141$	$0.187 \pm 0.041$	$0.707 \pm 0.146$	3.20e-231	1.38e-149	2.20e-257	2.78e-91
S3Diff	H.265	0.20	$27.12 \pm 3.77$	$0.331 \pm 0.133$	$0.176 \pm 0.040$	$0.737 \pm 0.144$	$26.77 \pm 3.62$	$0.311 \pm 0.132$	$0.158 \pm 0.038$	$0.731 \pm 0.143$	3.61e-158	5.34e-142	2.32e-250	8.97e-114
	11.203	0.23	$27.28 \pm 3.84$	$0.306 \pm 0.129$	$0.162 \pm 0.039$	$0.745 \pm 0.143$	$27.02 \pm 3.73$	$0.288 \pm 0.127$	$0.146 \pm 0.036$	$0.739 \pm 0.143$	1.51e-110	5.22e-125	7.66e-218	5.23e-112
-		0.35	$27.47 \pm 3.96$	$0.262 \pm 0.120$	$0.140\pm0.037$	$0.754 \pm 0.142$	$27.35 \pm 3.89$	$0.248\pm0.116$	$0.129 \pm 0.035$	$0.750 \pm 0.142$	1.06e-36	6.71e-96	8.88e-145	1.35e-83
		0.11	$27.18 \pm 3.87$	$0.342 \pm 0.135$	$0.180 \pm 0.038$	$0.737 \pm 0.146$	$26.79 \pm 3.73$	$0.320 \pm 0.132$	$0.157 \pm 0.034$	$0.731 \pm 0.145$	8.59e-150	6.47e-125	4.91e-261	2.61e-79
	Н 266	0.16	$27.39 \pm 3.93$	$0.305 \pm 0.128$	$0.160 \pm 0.037$	$0.748 \pm 0.144$	$27.16 \pm 3.84$	$0.288 \pm 0.125$	$0.142\pm0.034$	$0.743 \pm 0.143$	8.17e-96	7.37e-111	2.31e-232	1.12e-88
H.266	11.200	0.21	$27.48 \pm 3.97$	$0.280 \pm 0.122$	$0.147 \pm 0.036$	$0.754 \pm 0.143$	$27.33 \pm 3.91$	$0.265 \pm 0.119$	$0.133 \pm 0.034$	$0.749 \pm 0.143$	4.76e-62	2.01e-107	1.08e-199	2.13e-83
	0.26	$27.53 \pm 4.00$	$0.262 \pm 0.118$	$0.137 \pm 0.035$	$0.757 \pm 0.142$	$27.41 \pm 3.95$	$0.247 \pm 0.113$	$0.126 \pm 0.034$	$0.752 \pm 0.142$	2.02e-44	5.65e-109	2.91e-172	1.50e-82	

Table S4. S3Diff with and without VRPSR under x264 CRF rate-control on the Kodak dataset.

S3Diff         36         0.10         25.67         0.477         0.280         147.           S3Diff + VRPSR         36         0.10         25.23         0.439         0.253         113.           S3Diff         32         0.15         26.26         0.412         0.244         103.           S3Diff + VRPSR         32         0.15         25.94         0.382         0.220         77.           S3Diff         28         0.24         26.58         0.351         0.211         73.           S3Diff + VRPSR         28         0.24         26.46         0.331         0.190         62.4           S3Diff         26         0.35         26.69         0.322         0.193         59.4           S3Diff + VRPSR         26         0.35         26.60         0.303         0.175         53.							
S3Diff + VRPSR         36         0.10         25.23         0.439         0.253         113.           S3Diff         32         0.15         26.26         0.412         0.244         103.           S3Diff + VRPSR         32         0.15         25.94         0.382         0.220         77.           S3Diff         28         0.24         26.58         0.351         0.211         73.           S3Diff + VRPSR         28         0.24         26.46         0.331         0.190         62.4           S3Diff         26         0.35         26.69         0.322         0.193         59.0           S3Diff + VRPSR         26         0.35         26.60         0.303         0.175         53.	Method	CRF	bpp	PSNR	LPIPS	DISTS	FID
S3Diff         32         0.15         26.26         0.412         0.244         103.           S3Diff + VRPSR         32         0.15         25.94         0.382         0.220         77.3           S3Diff         28         0.24         26.58         0.351         0.211         73.3           S3Diff + VRPSR         28         0.24         26.46         0.331         0.190         62.4           S3Diff         26         0.35         26.69         0.322         0.193         59.4           S3Diff + VRPSR         26         0.35         26.60         0.303         0.175         53.2	S3Diff	36	0.10	25.67	0.477	0.280	147.46
S3Diff + VRPSR         32         0.15         25.94         0.382         0.220         77.3           S3Diff         28         0.24         26.58         0.351         0.211         73.3           S3Diff + VRPSR         28         0.24         26.46         0.331         0.190         62.4           S3Diff         26         0.35         26.69         0.322         0.193         59.4           S3Diff + VRPSR         26         0.35         26.60         0.303         0.175         53.2	S3Diff + VRPSR	36	0.10	25.23	0.439	0.253	113.60
S3Diff         28         0.24         26.58         0.351         0.211         73.3           S3Diff + VRPSR         28         0.24         26.46         0.331         0.190         62.4           S3Diff         26         0.35         26.69         0.322         0.193         59.4           S3Diff + VRPSR         26         0.35         26.60         0.303         0.175         53.2	S3Diff	32	0.15	26.26	0.412	0.244	103.38
S3Diff + VRPSR       28       0.24       26.46       0.331       0.190       62.0         S3Diff       26       0.35       26.69       0.322       0.193       59.0         S3Diff + VRPSR       26       0.35       26.60       0.303       0.175       53.3	S3Diff + VRPSR	32	0.15	25.94	0.382	0.220	77.81
S3Diff         26         0.35         26.69         0.322         0.193         59.0           S3Diff + VRPSR         26         0.35         26.60         0.303         0.175         53.0	S3Diff	28	0.24	26.58	0.351	0.211	73.89
S3Diff + VRPSR 26 0.35 26.60 0.303 0.175 53.3	S3Diff + VRPSR	28	0.24	26.46	0.331	0.190	62.61
	S3Diff	26	0.35	26.69	0.322	0.193	59.08
BDBR - 19.36% -18.41% -27.61% -30.1	S3Diff + VRPSR	26	0.35	26.60	0.303	0.175	53.25
		BDBR	_	19.36%	-18.41%	-27.61%	-30.10%